Heteroatom Chemistry
Volume 13, Number 6, 2002

Intermetallic Lithium Compounds with Two- and Three-Dimensional Polyanions—Synthesis, Structure, and Lithium Mobility

Rainer Pöttgen,[1] Zhiyun Wu,[1] Rolf-Dieter Hoffmann,[1] Gunter Kotzyba,[3] Henning Trill,[2] Jürgen Senker,[3] Dirk Johrendt,[4] Bernd D. Mosel,[2] and H. Eckert[2]

[1]*Institut für Anorganische und Analytische Chemie and SFB 458, Westfälische Wilhelms-Universität Münster, Wilhelm-Klemm-Straße 8, 48149 Münster, Germany*

[2]*Institut für Physikalische Chemie and SFB 458, Westfälische Wilhelms-Universität Münster, Schlossplatz 4/7, 48149 Münster, Germany*

[3]*Department Chemie, Ludwig-Maximilians-Universität München, Butenandtstraße 5-13 (Haus D), 81377 München, Germany*

[4]*Institut für Anorganische Chemie und Strukturchemie, Lehrstuhl II, Heinrich-Heine-Universität Düsseldorf, Universitätsstrasse 1, D-40225, Düsseldorf, Germany*

Received 25 March 2002

ABSTRACT: *Intermetallic lithium compounds are potential candidates as anode materials for battery applications. We report on the synthesis, crystal structures, and chemical bonding of lithium–transition metal–stannides and indides. These structures are composed of two- or three-dimensionally infinite polyanions formed by the transition metal and tin (indium) atoms. Besides the crystal chemistry we report on magnetic properties, ^{7}Li solid state NMR, and ^{119}Sn Mössbauer spectroscopy data in order to elucidate structure-property relations for this family of intermetallics.* © 2002 Wiley Periodicals, Inc. Heteroatom Chem 13:506–513, 2002; Published online in Wiley InterScience (www.interscience.wiley.com). DOI 10.1002/hc.10095

Correspondence to: Rainer Pöttgen; e-mail: pottgen@uni-muenster.de.

Contract grant sponsor: Fonds der Chemischen Industrie.
Contract grant sponsor: Deutsche Forschungsgemeinschaft.
Contract grant number: SFB 458.

INTRODUCTION

Lithium-based battery materials enable the development of cells with potentials up to 4 V, which can store large amounts of energy [1]. A sudden energy burst might cause local heating to high temperatures. This causes problems if the temperature rises above the melting point of lithium (454 K) when elemental lithium is used as anode material. Also the *shape change* of lithium anodes is puzzling. The reduced lithium may grow in the form of dendrites, fibers, and whiskers during the electrodeposition process, probably causing disconnection and electrical insulation or even electrical shortening between the electrodes.

Such problems can be avoided by using binary or ternary intermetallic lithium compounds, which have higher melting points. The intermetallics, however, carry two disadvantages: (i) because of the alloying element the density increases and (ii) the lithium activity decreases.

So far, only the phase diagrams of the binary systems are well established [2,3]. Most

studies concerning thermodynamic properties, the potential-composition correlation, ^{119}Sn Mössbauer spectroscopy, and chemical bonding [4–7, and ref. therein] were performed in the lithium–tin system. It is characterized by the intermetallics $Li_{17}Sn_4$ (formerly $Li_{22}Sn_5$), $Li_{13}Sn_5$, Li_7Sn_3, Li_7Sn_2, Li_5Sn_2, LiSn, and Li_2Sn_5 [8–14]. In combination with a transition metal (*T*), so far only few ternary stannides Li_2TSn and LiT_2Sn with cubic structures have been reported [15–22].

We have started a more systematic investigation of the lithium–transition metal–tin systems with respect to structure property relations. An overview of the recent results is presented herein.

EXPERIMENTAL

Synthesis

Lithium–transition metal–stannides and indides can be prepared in quantitative yield from the elemental components in sealed inert metal tubes (niobium or tantalum). Lithium is used in the form of rods in order to reduce the reactive surface. Reaction with moist air causes contaminations with LiOH and Li_3N in the form of a dark cusp at the surface. The noble metals were used as thin wires (Ø 1–2 mm) or powders (typically 200 mesh). Indium and tin were taken in the form of teardrops or granules. Lithium pieces were mixed with the noble metals and indium (tin) in the stoichiometric ratios and arc-welded in niobium or tantalum tubes [23] under an argon pressure (purified over titanium sponge at 900 K, silica gel and molecular sieves) of about 800 mbar. The sealed metal tubes were subsequently enclosed in evacuated silica tubes to prevent oxidation and then annealed in tube furnaces. Alternatively the metal tubes can be heated in a water-cooled sample chamber of a high-frequency furnace [24]. The samples can be separated quantitatively from the tubes. No reaction of the samples with the container material was observed. The compounds were stable in air over several weeks. For further details refer to the original papers.

Inductively Coupled Plasma—Atomic Emission Spectrometry Analyses

Besides the heavy noble metals it is difficult to get reliable values for the lithium content from the X-ray data. In most cases we have analyzed polycrystalline pieces of the lithium compounds by inductively coupled plasma–atomic emission spectrometry (ICP-AES) [25] using a VARIAN VISTA RL CCD Simultaneous ICP-AES. The samples were dissolved in a mixture of nitric and sulfuric acid (Merck, p.a.) using 40 ml teflon autoclaves and a MLS-ETHOS-PLUS microwave generator. No tantalum or niobium contaminations from the crucibles were observed.

X-Ray Investigations

The purity of the samples was checked by X-ray powder diffraction (Stoe StadiP powder diffractometer, Cu $K\alpha_1$ radiation) and the lattice parameters (see Table 1) were obtained from least-squares fits of the powder data. In the case of a larger range of homogeneity the lattice parameters of the single crystals are reported in Table 1. Single crystal intensity data of suitable single crystals were collected at room temperature by making use of a four-circle diffractometer (CAD4) or a Stoe image plate system with graphite monochromatized Mo K_α radiation.

TABLE 1 Crystal Data of Various Lithium–Transition Metal–Stannides and Indides

Compound	*Space Group*	*Structure Type*	*a (pm)*	*b (pm)*	*c (pm)*	*Residual*	*Reference*
$LiCoSn_6$	*Ibca*	$LiCoSn_6$	620.2 (1)	621.0 (1)	3699.6 (7)	0.024	This work
$LiPd_2Sn_6$	*P*4/*mbm*	$LiPd_2Sn_6$	663.92 (9)	*a*	843.2 (2)	0.050	[26]
$LiRuSn_4$	*I*4/*mcm*	$PdGa_5$	662.61 (3)	*a*	1116.98 (7)	0.073	[26,27]
$LiRhSn_4$	*I*4/*mcm*	$PdGa_5$	658.73 (5)	*a*	1136.4 (1)	0.053	[26,27]
$LiIrSn_4$	*I*4/*mcm*	$PdGa_5$	657.34 (5)	*a*	1130.4 (1)	0.034	[26,27]
$LiRh_3Sn_5$	*Pbcm*	$LiRh_3Sn_5$	537.4 (5)	977.7 (8)	1276 (1)	0.042	This work
$Li_3Pt_2Sn_3$	*Ia*3	$Li_3Pt_2Sn_3$	1263.9 (1)	*a*	*a*	0.018	This work
LiAuSn	*P*6$_3$/*mmc*	ZrBeSi	467.08 (8)	*a*	603.7 (1)	0.040	[28]
$LiAu_3Sn_4$	*P*6$_3$*mc*	$LiAu_3Sn_4$	448.31 (6)	*a*	2055.7 (4)	0.081	[28]
$Li_{1.86}RhIn_{1.14}$	*Fm*3*m*	BiF_3	631.8 (1)	*a*	*a*	0.047	This work
LiRhIn	*Fm*3*m*	BiF_3	644.0	*a*	*a*	–	[29]
$LiPdIn_2$	*Fm*3*m*	BiF_3	648.22 (5)	*a*	*a*	0.018	This work
$LiPdIn_2$	*Fm*3*m*	BiF_3	649.0	*a*	*a*	–	[29]
$LiPtIn_2$	*Fm*3*m*	BiF_3	646.10 (7)	*a*	*a*	0.018	This work
$LiPtIn_2$	*Fm*3*m*	BiF_3	645.9	*a*	*a*	–	[29]

Chemical Bonding Analysis

Self-consistent band structure calculations for $LiRuSn_4$ were performed using the LMTO method in its scalar-relativistic version (program TB-LMTO-ASA) [30]. Detailed descriptions are given elsewhere [31,32]. Reciprocal space integrations were performed with the tetrahedron method [33]. The basis sets consisted of 2s/2p/3d for Li, 5s/5p/4d for Ru, and 5s/5p/5d/4f for Sn. The 2p/3d orbitals of Li and 5d/4f of Sn were treated by the downfolding technique [34]. To achieve space filling within the atomic sphere approximation, interstitial spheres were introduced to avoid too large overlap of the atom-centered spheres. The COHP (Crystal Orbital Hamilton Population) method was used for the bond analysis [35].COHP gives the energy contributions of all electronic states for a selected bond. The values are negative for bonding and positive for antibonding interactions. With respect to the well-known COOP diagrams, we plot –COHP(E) to get positive values for bonding states.

Physical Property Measurements and Spectroscopy

The magnetic susceptibilities of polycrystalline samples were determined with a MPMS *XL* SQUID magnetometer (Quantum Design) in the temperature range of 4.2–300 K with magnetic flux densities up to 5 T. The ^{119}Sn Mössbauer spectroscopic investigations were carried out with a $Ca^{119m}SnO_3$ source. The measurements were performed in the usual transmission geometry in a commercial helium bath cryostat in the temperature range of 4.2–300 K. ^{7}Li solid state NMR spectroscopy was conducted at 155.5 MHz, on a Bruker DSX-400 spectrometer. Powdered samples diluted with silica were spun at 25 kHz in a 2.5-mm MAS probe. The 90° pulse length and relaxation delays were 2 μs and 4 s, respectively.

RESULTS AND DISCUSSION

Crystal Chemistry and Chemical Bonding

A common structural motif of the lithium–transition metal–stannides is the formation of polyanionic networks by the transition metal and tin atoms. These networks can have a more pronounced 2-D character or they are 3-D. In the case of 2-D networks, the lithium atoms separate them, while they occupy cavities within the 3-D ones. In the discussion of the crystal chemistry we will start with the pronounced 2-D polyanions.

The tetragonal stannides Li*T*Sn_4 (*T* = Ru, Rh, Ir) [27] (space group *I*4/*mcm*) crystallize with an ordered variant of the $PdGa_5$ type [36–39]. The transition-metal atoms have a square-antiprismatic tin coordination. These square anti-prisms are condensed via common faces forming 2-D [*T*Sn_4] polyanions which are separated by the lithium atoms (Fig. 1). Each lithium atom has a nearest-neighbor environment of eight tin atoms in the form of slightly compressed cubes. Similar distorted cubes occur already in the binary lithium stannides [13] and plumbides [40–44]. The various coordination polyhedra have been summarized by Frank and Müller [13]. In the case of elemental *bcc* lithium [45], the cube center and the corners are occupied by lithium, resulting in a $LiLi_{8/8}$ coordination. In the binary stannides several of the corners can be occupied by tin atoms. In the case of Li*T*Sn_4 (*T* = Ru, Rh, Ir) we find a $LiSn_{8/8}$ coordination with Li—Sn distances of 292 pm ($LiRuSn_4$) and 291 pm ($LiRhSn_4$ and $LiIrSn_4$). The Ru—Sn, Rh—Sn, and Ir—Sn distances of 279, 280, and 280 pm, respectively, within the 2-D [*T*Sn_4] polyanions are slightly larger than the sum of the covalent radii [46] of 265 pm (Ru + Sn/Rh + Sn) and 266 pm (Ir + Sn). Similar distances occur in the various binary transition-metal stannides. The various Sn—Sn distances in the Li*T*Sn_4 stannides range from 294 to 352 pm, similar to those in the β-tin structure (4 × 302 and 2 × 318 pm) [45]. Based on these distances we also expect a significant degree of Sn—Sn bonding besides strong *T*—Sn bonding. The shortest Sn—Sn distances of 300 pm (in $LiRuSn_4$) occur between the *T*Sn_8 square antiprisms where we observe slightly elongated Sn_4 tetrahedra with point symmetry $\bar{4}$. Such tetrahedra are also the building units in the rhodium-based stannide $LiRh_3Sn_5$ (see later).

The results of a DFT-LDA band structure calculation confirm this picture of chemical bonding for $LiRuSn_4$. Figure 2 shows the electronic density of states (DOS) together with the projections of states from lithium, tin, and ruthenium. No energy gap discerns at the Fermi level, where the DOS is dominated by tin and, to a lower extent, ruthenium states. $LiRuSn_4$ is clearly expected to be metallic. Although the lithium contribution to the DOS is small (Fig. 2), we find some occupation of Li states. From this we assume a positively polarized $Li^{\delta+}$, which transfers charge to the $[RuSn_4]^{\delta-}$ polyanions, but lithium is certainly not completely ionized.

As seen from the COHP diagrams in Fig. 3, the strongest bonds result from the Ru–Sn interaction and the corresponding bonding states are completely filled. This is not the case for the Sn—Sn bonds, whose bonding energy (ICOHP) is roughly 50% of a Ru—Sn bond. Thus, Sn—Sn bonding is likewise significant

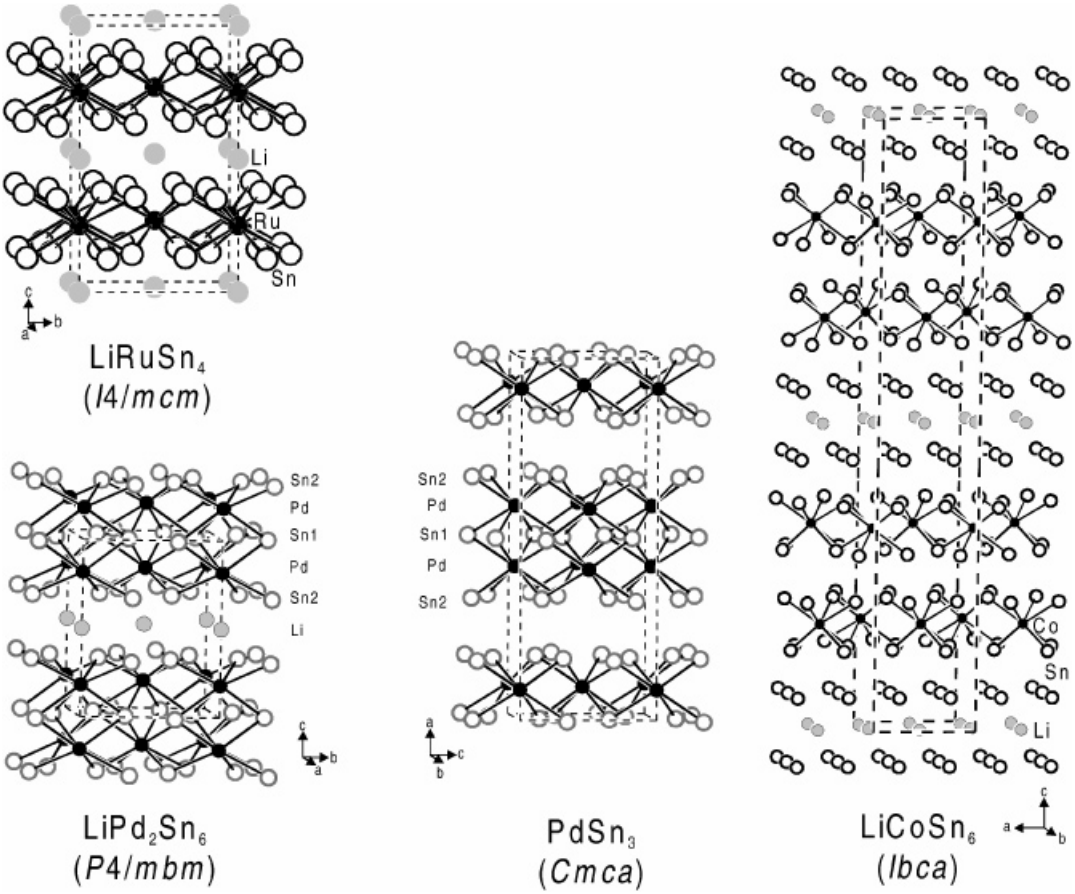

FIGURE 1 The crystal structures of $LiRuSn_4$, $LiPd_2Sn_6$, $LiCoSn_6$, and $PdSn_3$. Lithium, transition metal, and tin atoms are drawn as gray, black, and open circles, respectively. The 2-D polyanionic networks are emphasized. Note that the scaling varies for $LiCoSn_6$.

in $LiRuSn_4$ and would be slightly increased by higher valence electron counts, as expected for $LiRhSn_4$.

With palladium as the transition-metal component the stannide $LiPd_2Sn_6$ (space group *P*4/*mbm*) was obtained (Fig. 1) [26]. In this structure we also observe a square anti-prismatic tin coordination for the palladium atoms, however, now two [$PdSn_4$] layers are condensed via common tin atoms forming the 2-D [Pd_2Sn_6] polyanion. This structural motif directly derives from the structure of binary $PdSn_3$ [36]. Again, the lithium atoms have a square-prismatic tin coordination.

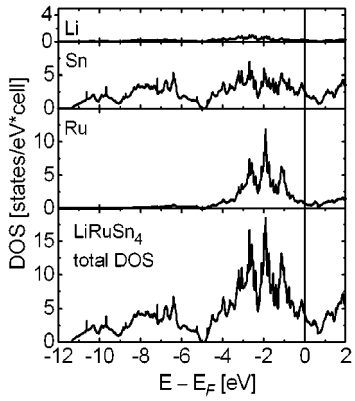

FIGURE 2 Electronic DOS of $LiRuSn_4$ and the projected contributions of Li, Sn, and Ru, respectively.

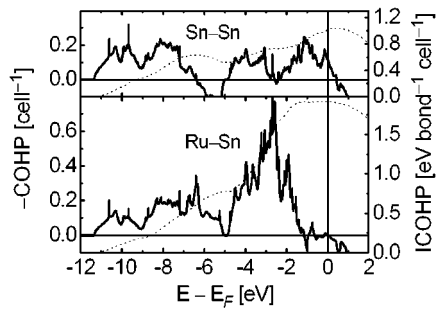

FIGURE 3 Sn—Sn and Ru—Sn COHP of $LiRuSn_4$. Dotted lines: COHP integrations.

In $LiPd_2Sn_6$ the Pd—Sn distances also compare well with the sum of the covalent radii. In contrast to the Li*T*Sn_4 stannides, $LiPd_2Sn_6$ shows a small range of homogeneity. The lithium position is occupied by 10% with palladium and one tin site has about 22% lithium occupancy, leading to a refined composition $Li_{1.35(1)}Pd_{2.10(1)}Sn_{5.56(1)}$ for the single crystal investigated.

The most complicated structure so far in this family of compounds is $LiCoSn_6$ (Fig. 1). This orthorhombic stannide crystallizes in the space group *Ibca* with very similar lattice parameters *a* and *b*, faking tetragonal symmetry. The cobalt atoms have a square anti-prismatic tin coordination and the lithium atoms fill square prisms. Along the relatively long *c* axis, we observe a stacking of one Li_2Sn_4 block followed by two $CoSn_4$ blocks resulting in the composition $Li_2Co_2Sn_{12} \equiv LiCoSn_6$. All blocks are connected via Sn—Sn bonding.

The structure of LiAuSn [28] (Fig. 4) contains planar hexagonal Au_3Sn_3 networks, which are separated by the lithium atoms. The Au—Sn distances within and between the Au_3Sn_3 networks are 270 and 302 pm, respectively. The gold and tin atoms both have a trigonal prismatic lithium coordination.

In $LiAu_3Sn_4$ the $[Au_3Sn_4]$ network is 3-D. As emphasized in Fig. 4, the structure can be described as an intergrowth of NiAs and $CaAl_2Si_2$ related slabs of compositions *AuSn* and $LiAu_2Sn_2$. The lithium atoms fill tetrahedral voids of gold atoms. These $LiAu_4$ tetrahedra point exclusively towards the +*z* direction classifying the structure as polar, space group $P6_3mc$.

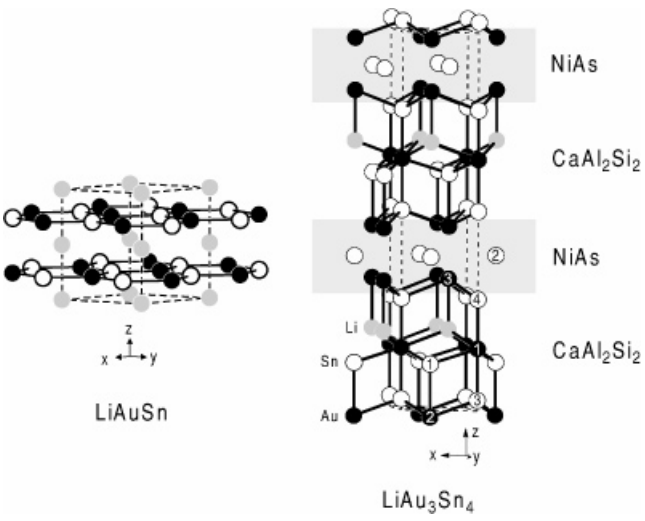

FIGURE 4 The crystal structures of LiAuSn and $LiAu_3Sn_4$. Lithium, gold, and tin atoms are drawn as gray, black, and open circles, respectively. The 2-D [AuSn] network of LiAuSn is emphasized. The $LiAu_3Sn_4$ structure is an intergrowth structure of NiAs (gray shading) and $CaAl_2Si_2$ related slabs.

The various Au—Sn distances (270–302 pm) compare well with the LiAuSn structure. Within the NiAs related slab of composition AuSn we observe Au—Au distances of 285 pm.

A complex 3-D $[Rh_3Sn_5]$ network occurs in $LiRh_3Sn_5$ (Fig. 5). Within this network, the lithium atoms fill larger voids of coordination number (CN) 13, formed by five rhodium and eight tin atoms. These CN13 polyhedra are connected via Sn—Sn bonds. Together, the tin atoms form a 3-D network with Sn—Sn distances ranging from 289 to 376 pm. Within this tin substructure we observe chains of trans edge-sharing $Sn_{4/2}$ tetrahedra.

Within the family of lithium intermetallics several compounds crystallize with structures related to the well-known fluorite type. The most complex superstructure within this series is certainly $Li_3Pt_2Sn_3$ (Fig. 6). With respect to the CaF_2 type, the $Li_3Pt_2Sn_3$ unit cell is doubled in all three directions. A slightly distorted CaF_2 related subcell of the platinum atoms is shown in the left-hand part of Fig. 6. The eight fluorine positions are occupied by two lithium and six tin atoms. Additionally we find lithium atoms in the octahedral voids formed by platinum. With respect to the fluorite structure we can write the formula as $Li[PtSn_{1.5}Li_{0.5}]$. This stannide shows a small range of homogeneity $Li_{3-x}Pt_2Sn_{3+x}$. So far two compositions have been verified through single crystal X-ray data: $x = 0.75$ and $x = 0.09$. We can thus consider these compounds as filled substitution variants of the binary stannide $PtSn_2$ [47] which itself adopts the fluorite type.

STRUCTURES OF INDIUM COMPOUNDS

The indium compounds $LiPdIn_2$ and $LiPtIn_2$ have already been reported by Schuster and coworkers [29] on the basis of X-ray powder data. We could grow

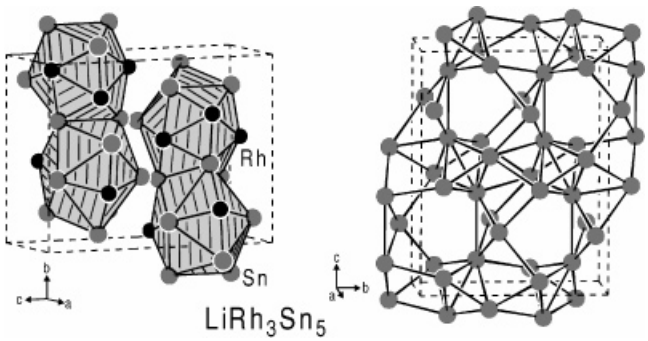

FIGURE 5 Crystal structure of $LiRh_3Sn_5$. The left-hand drawing emphasizes the CN13 polyhedra around the lithium atoms while the 3-D tin substructure is shown at the right-hand part.

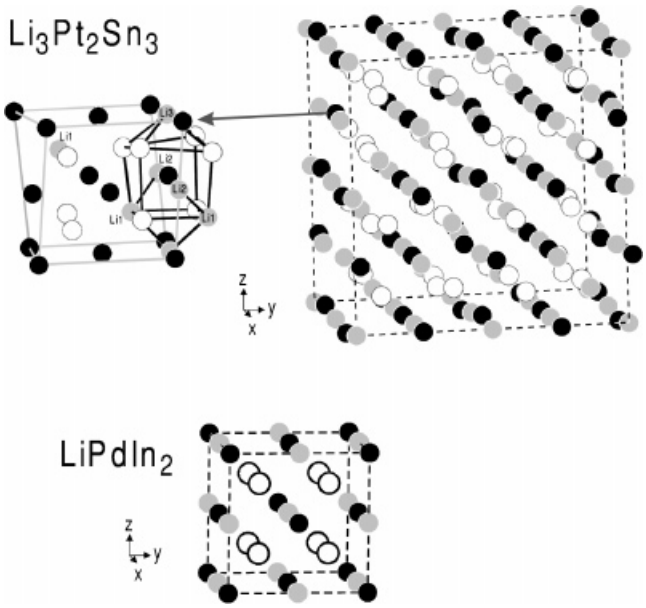

FIGURE 6 The crystal structures of $Li_3Pt_2Sn_3$ and $LiPdIn_2$. Lithium, transition metal, and tin (indium) atoms are drawn as gray, black, and open circles, respectively. For $Li_3Pt_2Sn_3$, one fluorite related subcell is outlined in the upper left-hand part.

small single crystals and refine the structures from single crystal diffractometer data. While $LiPdIn_2$ shows full occupancy for all atomic sites, we find lithium/indium mixing for the platinum compound, leading to the refined composition $Li_{0.75(1)}PtIn_{2.25(1)}$ for the single crystal investigated. Superstructure reflections indicating lithium/indium ordering have not been observed. Both structures may be described as lithium filled fluorite phases $PtIn_2$ and $PdIn_2$. At this point it is worthwhile to note that a binary compound $PdIn_2$ is not known in the palladium/indium system. It can only be stabilized by the addition of lithium. The electronic nature of this phenomenon is not yet understood.

With rhodium as the transition-metal component we obtained $Li_{1.86(1)}RhIn_{1.14(1)}$. This compound has the same atomic positions as $LiPdIn_2$ and $Li_{0.75(1)}PtIn_{2.25(1)}$, however, a higher lithium content. Also in the rhodium/indium system, a binary compound $RhIn_2$ is not known. In these fluorite related systems, ordered ternary compounds of compositions Li_2T In, LiT_2In, and LiT In_2 are possible. Thus, various solid solutions with lithium/indium mixing may occur. More detailed investigations of these systems are currently in progress.

Physical Properties and Spectroscopy

Several lithium compounds have been studied intensively with respect to their physical properties. As an example we present the data for $LiRuSn_4$. The temperature dependence of the magnetic susceptibility is displayed in Fig. 7. Over the whole temperature range we observe negative, nearly temperature independent susceptibilities with a room temperature value of -5.7×10^{-9} m^3/mol. This behavior is compatible with Pauli paramagnetism. Since the intrinsic diamagnetic contributions are large and the Pauli contribution is small, we still observe negative susceptibilities over the whole temperature range.

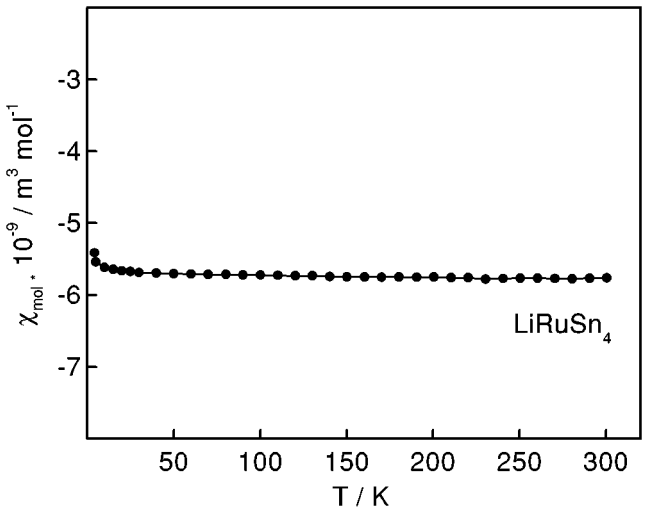

FIGURE 7 Temperature dependence of the magnetic susceptibility of $LiRuSn_4$ measured at an external magnetic flux density of 1 T.

A ^{119}Sn Mössbauer spectrum of $LiRuSn_4$ at 4.2 K is shown in Fig. 8. In agreement with the single crystallographic tin position we observe only one signal at an isomer shift $\delta = 2.21(4)$ mm/s, an experimental line width $\Gamma = 0.92(4)$ mm/s and a quadrupole splitting parameter $\Delta E_Q = 1.02(5)$ mm/s. The large quadrupole splitting results from the low site symmetry (..*m*) of the tin atoms. The rhodium and iridium compound show similar behavior.

In Fig. 9 we present a room temperature MAS NMR spectrum of $LiRuSn_4$, acquired at a spinning

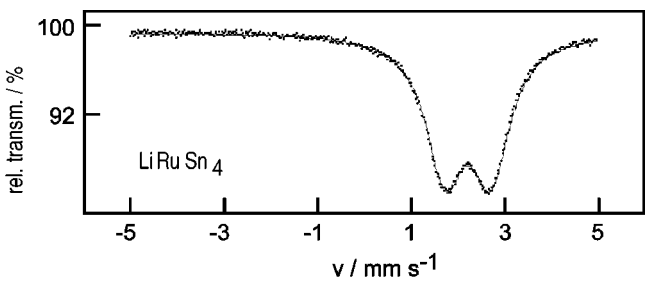

FIGURE 8 ^{119}Sn Mössbauer spectrum of $LiRuSn_4$ at room temperature.

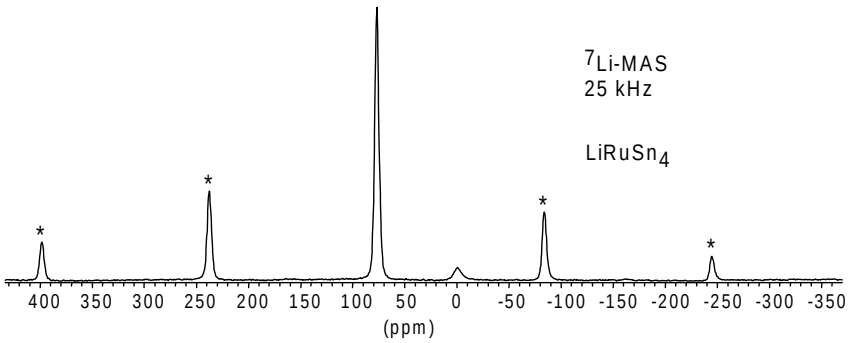

FIGURE 9 ^{7}Li MAS-NMR spectrum of $LiRuSn_4$ at room temperature. The peak at 0 ppm arises from an oxidic impurity. The asterisks mark spinning sidebands.

speed of 25 kHz. The isotropic chemical shift of 76.7 ppm vs. aqueous LiCl solution indicates a significant amount of delocalized s-electron density at the ^{7}Li nuclear site, resulting in a substantial Knight shift contribution. In contrast, the resonance shifts of the rhodium and iridium compounds are substantially smaller (14.5 and 9.5 ppm, respectively), indicating a much more ionic lithium site in the latter two compounds. Similar differences can also be inferred from spin-lattice relaxation time measurements. Preliminary temperature dependent studies conducted on static samples indicate the onset of motional narrowing due to lithium diffusion at temperatures exceeding 400 K.

ACKNOWLEDGMENTS

We are indebted to H. Hartl (LMU München) for the ICP-AES measurements, to Dipl.-Ing. U. Ch. Rodewald (WWU Münster), Dr. H. Piotrowski, and Dr. P. Mayer (both LMU München) for the single crystal data collections and the Degussa-Hüls AG for a generous gift of noble metals.

REFERENCES

[1] Huggins, R. A. In Handbook of Battery Materials; J. O. Besenhard (Ed.); Wiley-VCH: Weinheim, 1999.
[2] Villars, P.; Calvert, L. D. Pearson's Handbook of Crystallographic Data for Intermetallic Compounds; American Society for Metals: Materials Park, OH; 2nd edn., 1991; desk edition, 1997.
[3] Moffat, W. G. The Handbook of Binary Phase Diagrams; Genium, Schenectady, 1990.
[4] Wen, C. J.; Huggins, R. A. J Electrochem Soc 1981, 128, 1181.
[5] Wen, C. J.; Huggins, R. A. J Solid State Chem 1980, 35, 376.
[6] Dunlap, R. A.; Small, D. A.; MacNeil, D. D.; Obrovac, M. N.; Dahn, J. R. J Alloys Compd 1999, 289, 135.
[7] Genser, O.; Hafner, J. Phys Rev B 2001, 63, 144204.
[8] Gladyshevskii, G.; Oleksiv, G. I.; Kripyakevich, P. I. Sov Phys Crystallogr 1964, 9, 338.
[9] Hansen, D. A.; Chang, L. J. Acta Crystallogr 1969, B25, 2392.
[10] Müller, W.; Schäfer, H. Z Naturforsch 1973, 28b, 246.
[11] Müller, W. Z Naturforsch 1974, 29b, 304.
[12] Frank, U.; Müller, W.; Schäfer, H. Z Naturforsch 1975, 30b, 1 and 6.
[13] Frank, U.; Müller, W. Z Naturforsch 1975, 30b, 316.
[14] Goward, G. R.; Taylor, N. J.; Souza, D. C. S.; Nazar, L. F. J Alloys Compd 2001, 329, 82.
[15] Schuster, H.-U. Naturwissenschaften 1966, 53, 360.
[16] Pauly, H.; Weiss, A.; Witte, H. Z Metallkd 1968, 59, 47.
[17] Schuster, H.-U.; Thiedemann, D.; Schönemann, H. Z Anorg Allg Chem 1969, 370, 160.
[18] Kistrup, C.-J.; Schuster, H.-U. Z Naturforsch 1972, 27b, 324.
[19] Kistrup, C.-J.; Schuster, H.-U. Z Anorg Allg Chem 1974, 410, 113.
[20] Pobitschka, W.; Schuster, H.-U. Z Naturforsch 1978, 33b, 115.
[21] Eberz, U.; Seelentag, W.; Schuster, H.-U. Z Naturforsch 1980, 35b, 1341.
[22] Drews, J.; Eberz, U.; Schuster, H.-U. J Less-Common Met 1986, 116, 271.
[23] Pöttgen, R.; Gulden, Th.; Simon, A. GIT-Laborfachzeitschrift 1999, 43, 133.
[24] Pöttgen, R.; Lang, A.; Hoffmann, R.-D.; Künnen, B.; Kotzyba, G.; Müllmann, R.; Mosel, B. D.; Rosenhahn, C. Z Kristallogr 1999, 214, 143.
[25] Moore, G. L. Inductively Coupled Plasma–Atomic Emission Spectrometry; Elsevier: Amsterdam, 1989.
[26] Wu, Zh.; Hoffmann, R.-D.; Pöttgen, R. Z Kristallogr 2002, Suppl 19, 126.
[27] Wu, Zh.; Hoffmann, R.-D.; Pöttgen, R. Z Anorg Allg Chem, in press.
[28] Hoffmann, R.-D.; Johrendt, D.; Wu, Zh.; Pöttgen, R. J Mater Chem 2002, 12, 676.
[29] Czybulka, A.; Petersen, A.; Schuster, H.-U. J Less-Common Met 1990, 161, 303.
[30] Andersen, O. K.; Jepsen, O. Tight-Binding LMTO Vers. 47; Max-Planck-Institut für Festkörperforschung, Stuttgart, 1994.
[31] Jepsen, O.; Snob, M.; Andersen, O. K. Linearized Band Structure Methods and its Applications; Springer-Verlag: Berlin, 1987; Springer Lecture Notes.

[32] Skriver, H. L. The LMTO Method; Springer-Verlag, Berlin, 1984.
[33] Andersen, O. K.; Jepsen, O. Solid State Commun 1971, 9, 1763.
[34] Lambrecht, W. R. L.; Andersen, O. K. Phys Rev B 1986, 34, 2439.
[35] Dronskowski, R.; Blöchl, P. J Phys Chem 1993, 97, 8617.
[36] Schubert, K.; Lukas, H. L.; Meisner, H.-G.; Bhan, S. Z Metallkd 1959, 50, 534.
[37] Bhan, S.; Schubert, K. Trans Indian Inst Met 1960, 13, 332.
[38] Grin, Yu.; Peters, K.; von Schnering, H. G. Z Kristallogr 1997, 212, 6.
[39] Grin, Yu.; Wedig, U.; Wagner, F.; von Schnering, H. G.; Savin, A. J Alloys Compd 1997, 255, 203.
[40] Zalkin, A.; Ramsey, W. J. J Phys Chem 1958, 62, 689.
[41] Zalkin, A.; Ramsey, W. J. J Phys Chem 1956, 60, 234.
[42] Zalkin, A.; Ramsey, W. J.; Templeton, D. H. J Phys Chem 1956, 60, 1275.
[43] Nowotny, H. Z Metallkd 1941, 33, 388.
[44] Zalkin, A.; Ramsey, W. J. J Phys Chem 1957, 61, 1413.
[45] Donohue, J. The Structures of the Elements; Wiley: New York, 1974.
[46] Emsley, J. The Elements, 3rd ed.; Oxford University Press: New York, 1998.
[47] Charlton, J. S.; Cordey-Hayes, M.; Harris, I. R. J Less-Common Met 1970, 20, 105.